Dynamical optical tuning of the coherent phonon detection sensitivity in DBR-based GaAs optomechanical resonators

P. Sesin,[1] P. Soubelet,[1] V. Villafañe,[1] A. E. Bruchhausen,[1] B. Jusserand,[2] A. Lemaître,[3]
N. D. Lanzillotti-Kimura,[3] and A. Fainstein[1,*]

[1]*Centro Atómico Bariloche and Instituto Balseiro, C.N.E.A., 8400 S. C. de Bariloche, R. N., Argentina*
[2]*Institut des NanoSciences de Paris, UMR 7588 C.N.R.S.–Université Pierre et Marie Curie, 75015 Paris, France*
[3]*Laboratoire de Photonique et de Nanostructures, C.N.R.S., 91460 Marcoussis, France*

(Received 29 May 2015; published 11 August 2015)

We present a detailed time-resolved differential reflectivity study of the electronic and the coherent phonon generation response of a GaAs optical microcavity after resonant picosecond laser pulse excitation. A complex behavior is observed as a function of laser–cavity-mode detuning and incident power. The observed response is explained in terms of the large dynamical variations of the optical cavity-mode frequency induced by the ultrafast laser excitation, related to the optical modulation of the GaAs-spacer index of refraction due to photoexcited carriers. It is demonstrated that this effect leads to a strong optical dynamical tuning of the coherent phonon detection sensitivity of the device.

DOI: 10.1103/PhysRevB.92.075307 PACS number(s): 63.22.−m, 78.30.Fs, 78.67.Pt

I. MOTIVATION

Semiconductor optical microcavities based on distributed Bragg reflectors (DBRs) have received considerable attention in the last couple of decades, mainly due to the fascinating and rich physics of cavity polaritons in the strongly coupled regime [1–3], as single-photon emitters [4], and as the basis for the most efficient lasers, i.e., the vertical cavity surface emitting lasers (VCSELs) [5]. In the domain of phononics, microcavities have also been the subject of intense research. In the 1990s they were exploited for strongly enhanced (10^5–10^7) Raman scattering spectroscopy of phonons [6–9]. More recently they have been proposed as a means to amplify either the phonon generation, the detection, or both, in picosecond acoustics experiments [10,11]. Quite interestingly, it has also been shown that both passive and active microcavities can be strongly driven by externally injected acoustic pulses [12–18]. Surface acoustic waves generated with interdigited transducers have demonstrated strong modulation of the optical properties of microcavities both in the pure photonic [12] and strong coupling regimes [13,14]. In a conceptually similar scheme bulk propagating strains induced by femtosecond laser excitation of metal transducers deposited on the back side of the substrate have also been used to coherently drive planar microcavities [15,16] and, more recently, also VCSELs [17] and micropillar resonators [18]. We demonstrate here that *direct* laser pulse excitation of microcavities allows for the ultrafast optical tuning of the coherent phonon detection sensitivity of these devices.

It has been recently shown [19] that optical GaAs/AlAs-based microcavities constitute at the same time optimized resonators for near infrared light and for GHz-THz acoustic vibrations [20]. The potentiality of these structures in the field of cavity optomechanics [21–24] has been evidenced [19]. Cavity optomechanical phenomena (light-induced rigidity, optomechanical cooling, and optomechanical self-oscillation) could be thus integrated in these devices with optoelectronic phenomena as those described above (polariton physics, VCSELs, single-photon emitters, etc.). Besides the realization of simultaneous phonon-photon confinement, the direct and selective optical excitation of the cavity breathing modes [19,25,26] and the access to enormously enhanced optomechanical coupling of resonant photoelastic nature has been demonstrated in these structures [27].

In the context of these investigations a complex dynamics of the differential reflectivity induced by ultrafast laser pulses was reported [19]. Since electronic response and coherent phonon generation are intimately related in picosecond acoustics [28], it is the aim of this work to clarify the origin of the complex dynamics of electronic origin, and its relation to the coherent phonon signal. For this purpose detailed picosecond acoustics experiments as a function of cavity-laser detuning, and laser power, have been performed in a GaAs DBR microcavity. A phenomenological model based on the observed change of the index of refraction induced in bulk GaAs by picosecond-laser pulses is shown to explain well the microcavity experiments. The implications for the use of laser pulses for the optical tuning of the coherent phonon detection sensitivity in semiconductor optomechanical resonators is addressed.

II. SAMPLES AND EXPERIMENTAL SETUP

We consider a $\lambda/2$ GaAs-spacer planar vertical microcavity with DBRs of $Al_{0.18}Ga_{0.82}As$/AlAs layers, 20 pairs on the bottom, 18 on top, grown on a GaAs substrate. The structure performs as an optomechanical resonator that simultaneously confines photons and acoustic phonons of the same wavelength [19]. The sample had a small taper to allow for the tuning of the cavity-mode energy by displacing the laser spot on the sample surface.

Reflection-type pump-probe experiments [29] were performed at room temperature with λ_{laser} tuned around the optical cavity mode. The laser wavelength was set so that the phonon generation and detection would be close to resonance and slightly below the direct band gap of the GaAs making the cavity spacer ($E_{gap} \sim 1.425$ eV). The cavity experiments thus involve electronic resonances in the light-matter processes, in addition to the optical and acoustic resonances. This allows for a resonant enhancement of the optomechanical coupling,

*afains@cab.cnea.gov.ar

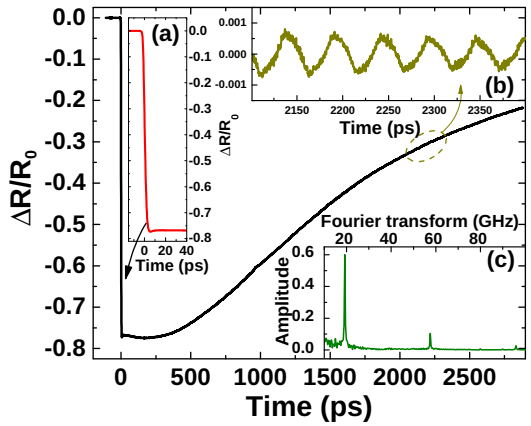

FIG. 1. (Color online) Typical differential reflectivity time trace. Panels (a)–(c) highlight the pump and probe coincidence and initial fast response, the modulation due to the generated coherent phonons, and the corresponding filtered Fourier transform, respectively.

while keeping low the absorption and high the cavity Q factor ($Q \sim 10^3$ in this case) [27]. Resonant coherent phonon generation experiments have been extensively used in the past for the study of layered semiconductor systems (see, for example, Refs. [30–32]) and for the selective excitation of confined acoustic vibrations in sound resonators [19,33]. Picosecond pulses (∼1 ps, ∼875 nm, ∼1.417 eV) from a mode-locked Ti:sapphire laser, repetition rate 80 MHz, were split into cross polarized pump (powers ranging from 10 to 100 mW) and probe (typically 1 mW) pulses. Photon pulses of 1 ps are chosen so that their spectral width matches the finesse of the optical cavity ($\Delta\lambda \sim 0.8$ nm). Both pulses were focused onto superimposed ∼50-μm-diameter spots.

The coupling of light to the microcavity was done as described in Refs. [34] and [35]. The probe is at normal incidence and is tuned close to the equilibrium high energy flank of the optical cavity mode by shifting the spot position on the sample. The pump pulse, at the same wavelength, is tuned resonant with the cavity mode. To this purpose a fine tuning of the pump pulse incidence angle is performed [10,34]. Once the angles of pump and probe pulses are set in this way, the detuning between laser and cavity mode can be varied by displacing the laser spot on the surface.

III. EXPERIMENTAL RESULTS

To proceed with the analysis and discussion of the measured differential reflectivity traces, we show in Fig. 1 a typical curve with its main features highlighted. A rapid response (panel a) characterizes the first few picoseconds ($t < 15$ ps), followed by a slower variation that covers several nanoseconds. These reflectivity variations originate in the change of index of refraction induced by electrons excited from the valence to the conduction band [28,36–38]. Based on previous investigations in GaAs bulk semiconductors, the initial response corresponding to the first few picoseconds, can be related to rapid hole and electron relaxation and carrier thermalization following photoexcitation [39–42]. The dynamics encompassing the following few nanoseconds is typically related to electron-hole recombination [43]. Most of the published studies in bulk materials have addressed these effects for above gap excitation, with only a few papers describing the transparency region [37,38]. In this latter case the observed effects derive mostly from residual disorder and temperature-induced absorption existent closely below the gap. However, a small electrostriction (Raman-like) contribution could also be present during the lifetime of the photon inside the cavity [28].

The same physical processes that contribute to the observed "electronic" differential reflectivity signal, lead to the coherent generation of phonons either through impulsive (electrostriction) or displacive (deformation potential and thermal) mechanisms [28,44]. The generated coherent vibrations in turn modulate the reflectivity, either through a photoelastic mechanism, or by the displacement of the structure interfaces. This can be observed in Fig. 1 as a fast harmonic contribution in the time domain (b), or through the filtered Fourier transform of the data (c).

Note that the used wavelength (875 nm) is well in the transparency region of the materials forming the DBRs, which have gaps higher than 1.62 eV (765 nm). Consequently, the phonon coherent generation (and the laser-induced change of index of refraction), and the photoelastic detection (change of refractive index induced by the phonon strain), both occur almost exclusively *at* the GaAs cavity spacer. In addition to the photoelastic detection mechanism one should consider the contribution due to the displacement of the interfaces, affecting the whole structure. However, it has been previously shown that at these wavelengths the photoelastic detection mechanism is dominant over the interface displacement one [19,33].

The right panel in Fig. 2 presents a selection of differential reflectivity traces [$\Delta R(t)/R_0$], as a function of time delay between pump and probe, obtained by setting the laser at 875 nm (pump and probe powers 100 and 2.5 mW, respectively), and varying the spectral detuning between the cavity mode and the laser by displacing the spot position on the wafer. The detuning is defined as $\Delta E = E_{\text{laser}} - E_{\text{cav}}$. Here E_{cav} is the energy of the cavity mode corresponding to the incidence angle of the probe beam. The detuning varies from top to bottom from $\Delta E = 4.6$ meV to $\Delta E = -4.7$ meV. At large positive detunings [see panel (a)], a small rapid positive component is observed at the coincidence between pump and probe, followed by a smoothly decreasing slow negative signal. A negative rapid component develops at positive detunings as soon as the pump energy starts to overlap with the cavity mode (b). This is accompanied by a more complex pattern of the slower component. The latter displays local minima that are detuning dependent [(c) and (d)]. The slow component then changes sign close to zero detuning [(d) and (e)]. Last, at extreme negative detunings again a small and positive rapid component develops. Globally $\Delta R(t)/R_0$ is large both at positive and negative detunings, with smaller values observed at $\Delta E \sim 0$ and at the extreme detunings. It is the purpose of this work to explain this seemingly complex behavior, and its relation to the efficiency for coherent phonon detection.

It should be realized that the observed laser-induced reflectivity changes, as large as 60%, are enormous. Indeed, typical variations in similar experiments performed on bulk GaAs amount to a few 10^{-3}. Such amplification arises both through a cavity-induced enhancement of the pump field

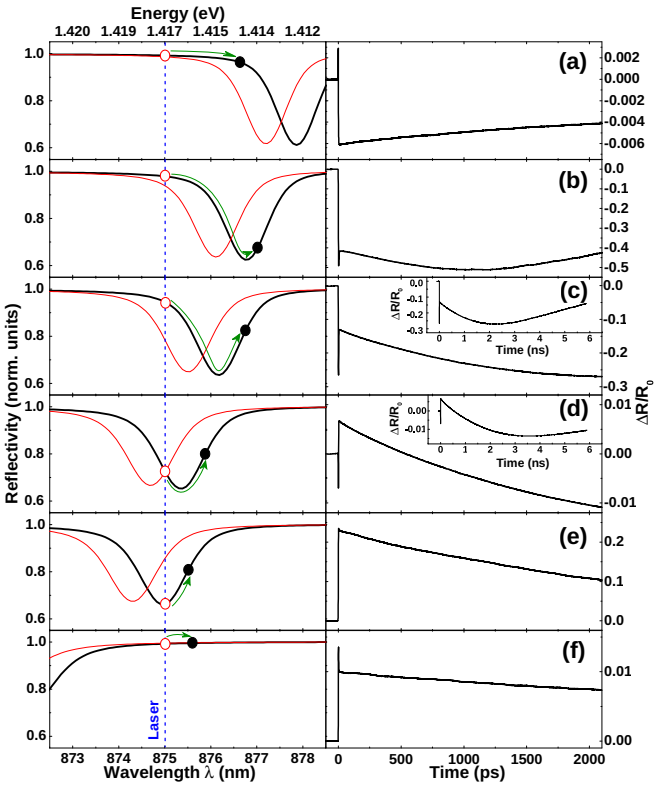

FIG. 2. (Color online) Right: Selected differential reflectivity traces. Insets in panels (c) and (d) provide details of the same curves at longer delay times. Left: Optical cavity modes sensed by pump (thin red curves) and probe (thick black curves) pulses at the same sample position as the corresponding differential reflectivity trace shown in the right panel. Arrows represent the relative displacement of the cavity mode with respect to the laser line after ultrafast laser excitation.

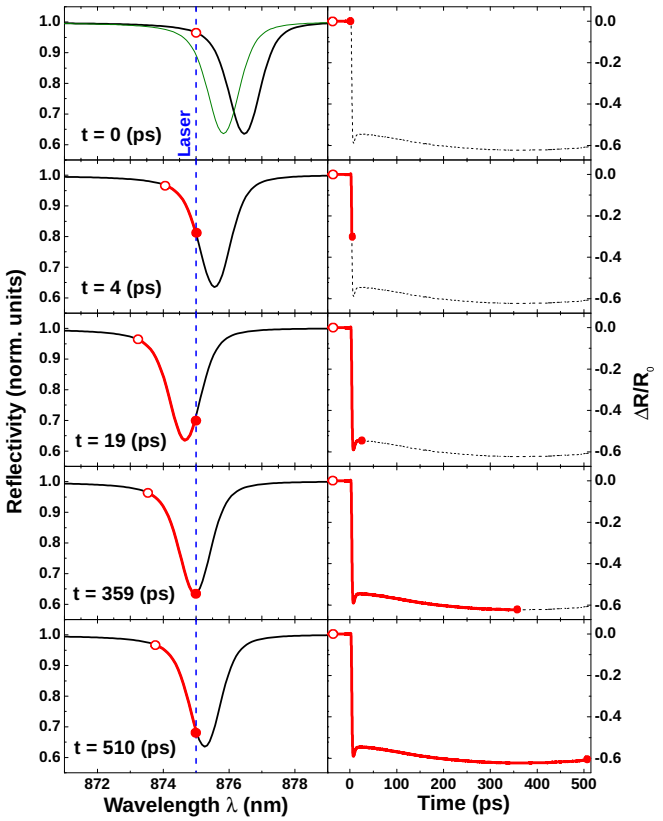

FIG. 3. (Color online) Schematic diagram representing different snapshots of the time evolution of the cavity mode sensed by the probe (thick black curves) after ultrafast laser excitation (left), together with the corresponding expected differential reflectivity signal (right). The thin green curve in the top panel is the cavity mode sensed by the pump.

at the spacer layer and a concomitant augmented carrier concentration at similar pump powers (generation process), and because of the cavity-induced appearance of a sharp reflectivity dip at the cavity mode (detection process). In fact, while bulk reflectivities have smooth spectral dependencies even at critical points, a Q factor of the order of 10^3 in a well designed DBR resonator implies changes of the order of 1 with wavelength variations of only fractions of nanometers.

As we will show next, the way the cavity mode is perturbed after a fast optical excitation is critical for the understanding of coherent phonon experiments in these structures. To this purpose we show in Fig. 2 (left panels) the spectral position of the optical cavity modes sensed both by the pump (thin curves) and probe pulses (thick curves), corresponding to the traces shown in the right panels. Calculated curves are shown, based on a cartography of the cavity modes obtained through photoluminescence measurements. We note that in some specific cases when the reflectivity sensed by the pump and probe pulses was measured, it agreed very well with the calculated curves. The wavelength of the laser is indicated in Fig. 2 with a vertical dashed line.

The way to understand the main features of the differential reflectivity traces in Fig. 2 is through a rapid blueshift of the cavity mode after ultrafast laser excitation, followed by a slow recovery of the equilibrium situation after carrier recombination. The arrows in the left panels of Fig. 2 indicate the estimated final relative position of the laser line and cavity mode, immediately after pump pulse excitation. Figure 3 provides a cartoon with several snapshots of how the cavity mode is changing with time, and the corresponding evolution of the differential reflectivity $\Delta R/R_0$ sensed by the probe, for the specific case (b) in Fig. 2. From the consideration of Figs. 2 and 3, several conclusions can be drawn: (i) as soon as the pump laser overlaps with the cavity mode, even at modest powers the cavity mode is made to rapidly blueshift by values of the order of its FWHM. (ii) Since the resonant condition is that the spacer thickness corresponds to half wavelength, $d = \lambda/2n_{\mathrm{GaAs}}$, with n_{GaAs} the GaAs index of refraction, a blueshift indicates a *decrease* of n_{GaAs} after carrier excitation. This is compatible with measurements performed on "bulk" GaAs [45], indicating a blueshift of the effective fundamental band gap, and consequently that band filling is more important than band-gap renormalization in the studied system and experimental conditions. (iii) The rapid negative dip arises from the passage of the cavity mode minimum through the laser energy immediately after pulse excitation. The local minima observed at longer times ($t > 15$ ps), which are dependent on detuning, describe the same passage in the opposite direction when the structure returns to equilibrium

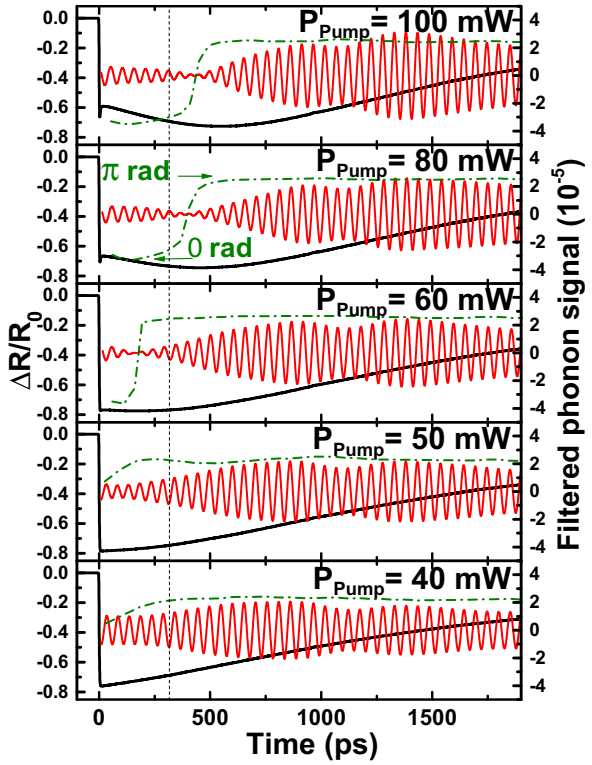

FIG. 4. (Color online) Differential reflectivity time traces for an initial positive detuning, as a function of pump pulse power (thicker black curves). The oscillating red traces are the corresponding filtered phonon induced reflectivity modulations, corresponding to the first breathing mode at ∼19 GHz (right axis). Dashed-dotted curves indicate the phonon signal phase. The observed π phase change with increasing pump power is further evidenced by the vertical thin dashed line.

after carrier recombination. This explains why for most of the cases, irrespective of detuning, the maximum value of ΔR is of the order of 0.6, the depth of the cavity mode. (iv) At the extremes of positive and negative studied detuning, the initial rapid response has a positive sign, something that cannot be explained within the presented description. It might be signaling a fast carrier-lattice thermalization transient, or the presence of an electrostriction contribution that is blurred out when the more intense deformation potential contribution comes into play once significant excited carriers are present. This point will be discussed further below.

One way to test the above picture is to set the probe energy above that of the cavity mode, and perform experiments as a function of pump power. This is illustrated with the thick curves in Fig. 4, for pump powers ranging from 40 to 100 mW. At the smaller powers a simple monotonous slow decay of $\Delta R/R_0$ is observed after pump excitation. Above ∼60 mW a rapid negative dip develops, accompanied by the related power dependent local minima in the slow recovery towards equilibrium. The interpretation is straightforward: at the smaller powers, the refractive index variations induced by carrier excitation is not sufficient to produce the cavity-mode–laser crossing for the chosen initial detuning, leading to a monotonous return to equilibrium. Mode crossing is observed above ∼60 mW. We note that if the angles of pump and probe are reversed, the

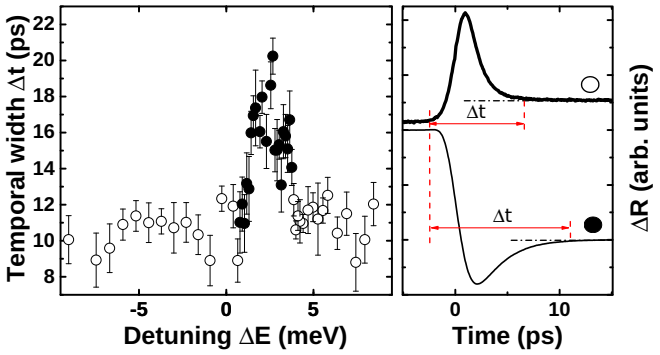

FIG. 5. (Color online) Left: Temporal width of the rapid component of the differential reflectivity traces presented in Fig. 2. Solid(empty) symbols correspond to negative(positive) features. Right: Definition of the temporal width, illustrated both with negative and positive cases.

observed general dynamics is qualitatively different. In fact, in this case when the pump is resonant with the cavity mode, the probe is tuned to the *lower* energy flank of the mode. Thus, a pump-induced blueshift of the mode always leads to the probe beam being out of resonance, and thus to monotonous decreasing weak signals. This was experimentally verified.

As argued above, the initial *negative* rapid feature observed in the differential time traces can be explained as due to the fast crossing of the cavity mode and the laser spectral position observed immediately after the pump-induced carrier excitation. What remains to be explained is the *positive* rapid signal observed at the extreme positive and negative detunings [see Figs. 2(a) and 2(f) for $t < 15$ ps]. We show in Fig. 5 the temporal width Δt of this initial feature, as a function of detuning, derived from time traces as those shown in Fig. 2. Since it is not possible to define unambiguously a FWHM for the rapid component of the time traces (particularly when rapid and slow components have different sign), we have chosen to show as Δt the full width elapsing from the onset of the coincidence, to the approximate time when only the differential reflectivity slow component remains. In Fig. 5 negative (positive) dips are distinguished with solid (open) symbols. It is quite notable that positive dips have all essentially the same time dynamics, which is shorter and markedly different from that of the negative dip described above. This supports our understanding that the two features have a different physical origin: the cavity-mode–laser crossing in the negative dip case (which would also exist if the refractive index change would simply behave like a step function), and a fast carrier relaxation induced transient in the positive case (which is probably blurred out in the presence of the larger negative feature). We note that in all cases the observed rapid components are significantly longer than the laser pulse width (∼1 ps FHWM), indicating that they reflect intrinsic properties of the index of refraction (and hence cavity-mode) dynamics. Dynamics lasting a few picoseconds could be compatible with a thermalization of the quasiequilibrium carriers with the lattice, which for such resonant excitation proceeds through the interaction with acoustic phonons.

Now that the qualitative behavior of the electronic component of the differential reflectivity signals has been established,

we turn our analysis to the coherent phonon signals. Irrespective of the main coherent phonon generation mechanism, it is to be expected that the coherent phonon signals follow the following dynamics:

$$\Delta R/R_0 \propto \cos(\Omega_{\text{phonon}} t) e^{-t/\tau} S(t), \tag{1}$$

where Ω_{phonon} is the involved coherently excited confined phonon frequency, and τ the phonon lifetime. $S(t)$ is a coherent phonon detection *sensitivity* function, reflecting the time dependent tuning of the probe pulse to different slopes of the cavity-mode resonance. In fact, as discussed in Ref. [34], the detected signal is proportional to the spectral derivative of the reflectivity sensed by the probe beam. Note that we assume a cosine time dependence appropriate for a displacive (deformation potential) generation mechanism. Note also that Eq. (1) implies that confined phonon lifetimes [46] *cannot* be straightforwardly derived from these ultrafast laser experiments without a proper description of $S(t)$.

To test the validity of Eq. (1) we show with the thinner curves in Fig. 4 the filtered phonon contributions to $\Delta R/R_0$ corresponding to the confined breathing mode at ~19 GHz [19], together with the as-measured differential reflectivity traces (thick curves). Gaussian filters to the first derivative of the traces have been used to extract the oscillatory signals. Quite notably, the phonon related traces show nontrivial time dependencies. Their amplitude can increase or decrease immediately after generation depending on the pump power, and can even have intensity nodes followed by signal recovery at finite delay times.

The observed complex time dependencies of the phonon amplitude can be naturally understood as due to the presence of $S(t)$ in Eq. (1). A node is expected to reflect the crossing of the cavity mode and laser energy (zero derivative of the reflectivity), while the signal increase or decrease will reflect the laser line approaching or departing from reflectivity minima (zero derivative) or reflectivity flanks (larger derivatives). Concomitant with a signal node related to a cavity-mode–laser crossing, the change of sign of the derivative of the reflectivity at zero detuning should lead to a phase slip by π in the oscillatory signal. In fact, on one side of the optical mode, a phonon modulating the index of refraction will produce a signal with a given sign, while on the other it will present the opposite sign, crossing a zero when the derivative of the reflectivity is zero. That this is indeed the case is shown with dashed-dotted curves in Fig. 4. The vertical thin dashed line in the figure is included to highlight maxima of the oscillations in the top traces that evolve into minima when the pump power is reduced.

To model the observed behavior we assume that the photoexcited carriers induce a change in the complex index of refraction $n(t) + i\kappa(t)$ of the GaAs spacer given by

$$\delta n(t) = \frac{\delta n_0}{2}\{1 + \text{erf}[(t - t_0)/\tau_t]\} e^{-(t-t_0)/\tau_{\text{rec}}}, \tag{2}$$

$$\delta \kappa(t) = \frac{\delta \kappa_0}{2}\{1 + \text{erf}[(t - t_0)/\tau_t]\} e^{-(t-t_0)/\tau_{\text{rec}}}. \tag{3}$$

Here τ_{rec} describes the time required to recover the equilibrium situation (essentially determined by the photocarrier recombination time), τ_t reflects the fast transient required to attain the quasiequilibrum state of the photoexcited carriers, and erf refers to the "error function." For each time dependent value of $n(t)$ and $\kappa(t)$, $\Delta R/R_0$ is evaluated using standard matrix methods, so that δn_0, $\delta \kappa_0$, τ_{rec}, and τ_t can be extracted from a least-square fit of the experimental time traces. We show in the top panel of Fig. 6 one example of such a fit, corresponding to one of the traces displayed in Fig. 2. The

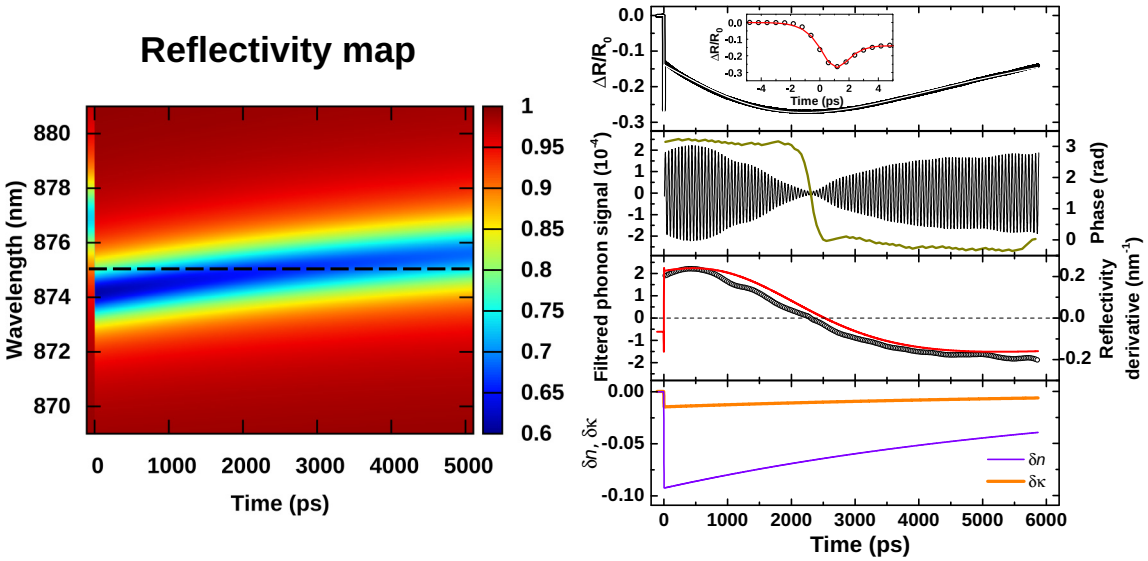

FIG. 6. (Color online) Left: Color map showing the calculated time evolution of the cavity-mode reflectivity after pump laser excitation. Note the change of position and depth of the mode. The horizontal dashed line corresponds to the laser wavelength. Right: The top panel shows the experimental (open symbols) and modeled (continuous light curve) differential reflectivity time trace. The inset shows a detail of the first rapid response. The middle top panel is the corresponding filtered phonon signal amplitude and phase. The middle bottom panel displays the phonon amplitude (open symbols) compared to the calculated sensitivity function $S(t)$. The latter is evaluated as the spectral derivative of the reflectivity $R(t)$ at the probe wavelength (see text for details). The bottom panel shows the derived $\delta n(t)$ (thin blue curve) and $\delta \kappa(t)$ (thick orange curve) used to calculate the left panel reflectivity, and the time trace shown in the top panel.

agreement is almost perfect, both for the fast (inset) and slow components, using as fitting parameters $\delta n_0 = -0.093$, $\delta\kappa_0 = -0.015$, $\tau_{\rm rec} = 6.8$ ns, and $\tau_t = 2.1$ ps. The values of $\delta n(t)$ and $\delta\kappa(t)$ used to derive the modeled time trace are shown in the bottom panel of the same figure. These are also used to calculate the time dependence of the reflectivity around the cavity mode, shown in the left panel of Fig. 6. Note (i) the rapid blueshift of the cavity mode after laser pump excitation, from ≈877 nm to ≈874 nm, essentially determined by a change in the real part of the refractive index, $\delta n(t)$, (ii) the initial improvement of the cavity mode Q factor induced by a negative $\delta\kappa(t)$ (reduced absorption), and (iii) the slow exponential return to equilibrium. The crossing of the mode with the horizontal dashed line (laser wavelength) leads to the two minima in the time trace shown in the top right panel in Fig. 6.

The top middle panel in Fig. 6 shows the filtered phonon signal, and its associated phase, for the differential reflectivity trace being analyzed. Again a nontrivial time dependence of the phonon signal's amplitude is observed, including a node and a π phase shift close to the minimum of the electronic $\Delta R/R_0$. The bottom middle panel shows the measured amplitude of the filtered phonon signal (open symbols), compared to the calculated sensitivity function $S(t)$ (continuous curve). For the measured amplitudes a change of sign has been assigned to account for the π change of phase at the node. $S(t)$ is calculated as the spectral derivative of the reflectivity shown in Fig. 6 (left), evaluated at the laser wavelength and at each time t. The agreement is quite remarkable, taking into account that only the magnitude of $S(t)$ has been adjusted to fit the initial maximum amplitude of the phonon signal. Besides this overall agreement, two more subtle features emerge that should be highlighted. First, the measured phonon signal does not decrease within the first 6 ns *faster* than $S(t)$. This means that the phonon lifetime of the 19 GHz cavity confined modes is significantly longer than the measured window even at room temperature [$e^{-t/\tau} \sim 1$ in Eq. (1)]. And second, we have systematically observed that the amplitude's nodes occur at shorter times (∼200–300 ps) when compared to the zero derivative of the electronic signal. While we still have no definitive explanation for this notable effect, we believe it might be related to the imaginary part of either the electronic induced change of the index of refraction [$\delta\kappa(t)$], or of the photoelastic constant [34].

IV. CONCLUSIONS

In conclusion, we have presented a detailed study of the time-resolved reflectivity modulation induced by direct ultrafast laser excitation of a GaAs semiconductor microcavity. Both the electronic and coherent phonon contributions to the differential reflectivity were analyzed, and their relation addressed. A very strong perturbation of the cavity mode upon laser direct excitation was evidenced, leading to a strong optical dynamical tuning of the coherent phonon detection sensitivity of the device. The presented investigation is relevant for the application of optical microcavities to ultrafast phonon modulated optoelectronic devices, and for the study of fundamental phenomena in cavity optomechanics. It should be interesting also to study the possibility to use the studied scheme for the determination of parameters relevant to photoelastic phenomena in semiconductors, namely, photoelastic constants and light-induced complex refractive index modulations. These parameters are poorly accessible, particularly below the absorption gap and at resonance, where most of the microcavity applications are expected to be relevant.

[1] A. Kavokin and G. Malpuech, *Cavity Polaritons* (Elsevier, Amsterdam, 2003).

[2] Semicond. Sci. Technol. **18**(10) (2003), special issue on microcavities, edited by J. J. Baumberg and L. Viña.

[3] E. Wertz, L. Ferrier, D. D. Solnyshkov, R. Johne, D. Sanvitto, A. Lemaître, I. Sagnes, R. Grousson, A. V. Kavokin, P. Senellart, G. Malpuech, and J. Bloch, Nat. Phys. **6**, 860 (2010).

[4] A. Dousse, J. Suffczyński, A. Beveratos, O. Krebs, A. Lemaître, I. Sagnes, J. Bloch, P. Voisin, and P. Senellart, (London) **466**, 217 (2010).

[5] T. Someya, Science **285**, 1905 (1999).

[6] A. Fainstein, B. Jusserand, and V. Thierry-Mieg, Phys. Rev. Lett. **75**, 3764 (1995).

[7] A. Fainstein, B. Jusserand, and V. Thierry-Mieg, Phys. Rev. Lett. **78**, 1576 (1997).

[8] A. Fainstein, B. Jusserand, and V. Thierry-Mieg, Phys. Rev. B **53**, R13287 (1996).

[9] A. Fainstein and B. Jusserand, Phys. Rev. B **57**, 2402 (1998).

[10] N. D. Lanzillotti-Kimura, A. Fainstein, A. Huynh, B. Perrin, B. Jusserand, A. Miard, and A. Lemaître, Phys. Rev. Lett. **99**, 217405 (2007).

[11] Y. Li, Q. Miao, A. V. Nurmikko, and H. J. Maris, J. Appl. Phys. **105**, 083516 (2009).

[12] M. M. de Lima, R. Hey, P. V. Santos, and A. Cantarero, Phys. Rev. Lett. **94**, 126805 (2005).

[13] M. M. de Lima, M. van der Poel, P. V. Santos, and J. M. Hvam, Phys. Rev. Lett. **97**, 045501 (2006).

[14] E. A. Cerda-Méndez, D. N. Krizhanovskii, M. Wouters, R. Bradley, K. Biermann, K. Guda, R. Hey, P. V. Santos, D. Sarkar, and M. S. Skolnick, Phys. Rev. Lett. **105**, 116402 (2010).

[15] A. V. Scherbakov, T. Berstermann, A. V. Akimov, D. R. Yakovlev, G. Beaudoin, D. Bajoni, I. Sagnes, J. Bloch, and M. Bayer, Phys. Rev. B **78**, 241302 (2008).

[16] T. Berstermann, A. V. Scherbakov, A. V. Akimov, D. R. Yakovlev, N. A. Gippius, B. A. Glavin, I. Sagnes, J. Bloch, and M. Bayer, Phys. Rev. B **80**, 075301 (2009).

[17] T. Czerniuk, C. Brüggemann, J. Tepper, S. Brodbeck, C. Schneider, M. Kamp, S. Höfling, B. A. Glavin, D. R. Yakovlev, A. V. Akimov, and M. Bayer, Nat Commun. **5**, 4038 (2014).

[18] T. Czerniuk, J. Tepper, A. V. Akimov, S. Unsleber, C. Schneider, M. Kamp, S. Höfling, D. R. Yakovlev, and M. Bayer, Appl. Phys. Lett. **106**, 041103 (2015).

[19] A. Fainstein, N. D. Lanzillotti-Kimura, B. Jusserand, and B. Perrin, Phys. Rev. Lett. **110**, 037403 (2013).

[20] M. Trigo, A. Bruchhausen, A. Fainstein, B. Jusserand, and V. Thierry-Mieg, Phys. Rev. Lett. **89**, 227402 (2002).
[21] O. Arcizet, P.-F. Cohadon, T. Briant, M. Pinard, and A. Heidmann, Nature (London) **444**, 71 (2006).
[22] T. J. Kippenberg and K. J. Vahala, Science **321**, 1172 (2008).
[23] M. Eichenfield, J. Chan, R. M. Camacho, K. J. Vahala, and O. Painter, Nature (London) **462**, 78 (2009).
[24] M. Aspelmeyer, T. J. Kippenberg, and F. Marquardt, Rev. Mod. Phys. **86**, 1391 (2014).
[25] N. Lanzillotti-Kimura, A. Fainstein, and B. Jusserand, Ultrasonics **56**, 80 (2015).
[26] S. Anguiano, G. Rozas, A. E. Bruchhausen, A. Fainstein, B. Jusserand, P. Senellart, and A. Lemaître, Phys. Rev. B **90**, 045314 (2014).
[27] G. Rozas, A. E. Bruchhausen, A. Fainstein, B. Jusserand, and A. Lemaître, Phys. Rev. B **90**, 201302 (2014).
[28] P. Ruello and V. E. Gusev, Ultrasonics **56**, 21 (2015), brief review of the physical mechanisms leading to the generation of coherent acoustic phonons by ultrafast laser action.
[29] C. Thomsen, H. T. Grahn, H. J. Maris, and J. Tauc, Phys. Rev. B **34**, 4129 (1986).
[30] A. Bartels, T. Dekorsy, H. Kurz, and K. Köhler, Phys. Rev. Lett. **82**, 1044 (1999).
[31] K. Mizoguchi, M. Hase, S. Nakashima, and M. Nakayama, Phys. Rev. B **60**, 8262 (1999).
[32] O. Matsuda and O. B. Wright, J. Opt. Soc. Am. B **19**, 3028 (2002).
[33] M. F. Pascual Winter, G. Rozas, A. Fainstein, B. Jusserand, B. Perrin, A. Huynh, P. O. Vaccaro, and S. Saravanan, Phys. Rev. Lett. **98**, 265501 (2007).
[34] N. D. Lanzillotti-Kimura, A. Fainstein, B. Perrin, and B. Jusserand, Phys. Rev. B **84**, 064307 (2011).
[35] N. D. Lanzillotti-Kimura, A. Fainstein, B. Perrin, B. Jusserand, L. Largeau, O. Mauguin, and A. Lemaitre, Phys. Rev. B **83**, 201103 (2011).
[36] E. N. Glezer, Y. Siegal, L. Huang, and E. Mazur, Phys. Rev. B **51**, 6959 (1995).
[37] P. Babilotte, E. Morozov, P. Ruello, D. Mounier, M. Edely, J.-M. Breteau, A. Bulou, and V. Gusev, J. Phys.: Conf. Ser. **92**, 012019 (2007).
[38] S. Kim, E. Oh, J. U. Lee, D. S. Kim, S. Lee, and J. K. Furdyna, phys. stat. sol. (c) **2**, 3141 (2005).
[39] W. H. Knox, C. Hirlimann, D. A. B. Miller, J. Shah, D. S. Chemla, and C. V. Shank, Phys. Rev. Lett. **56**, 1191 (1986).
[40] C. J. Stanton, D. W. Bailey, and K. Hess, Phys. Rev. Lett. **65**, 231 (1990).
[41] R. Tommasi, P. Langot, and F. Vallée, Appl. Phys. Lett. **66**, 1361 (1995).
[42] A. Alexandrou, V. Berger, and D. Hulin, Phys. Rev. B **52**, 4654 (1995).
[43] A. Amo, M. D. Martín, L. Viña, A. I. Toropov, and K. S. Zhuravlev, Phys. Rev. B **73**, 035205 (2006).
[44] S. Hunsche, H. Heesel, A. Ewertz, H. Kurz, and J. H. Collet, Phys. Rev. B **48**, 17818 (1993).
[45] Y. H. Lee, A. Chavez-Pirson, S. W. Koch, H. M. Gibbs, S. H. Park, J. Morhange, A. Jeffery, N. Peyghambarian, L. Banyai, A. C. Gossard, and W. Wiegmann, Phys. Rev. Lett. **57**, 2446 (1986).
[46] G. Rozas, M. F. Pascual Winter, B. Jusserand, A. Fainstein, B. Perrin, E. Semenova, and A. Lemaître, Phys. Rev. Lett. **102**, 015502 (2009).